npj | Quantum Materials

www.nature.com/npjquantmats

ARTICLE OPEN

Direct observation of the spin–orbit coupling effect in magnetic Weyl semimetal $Co_3Sn_2S_2$

D. F. Liu[1,2,13], E. K. Liu[3,4,13], Q. N. Xu[5,13], J. L. Shen[3], Y. W. Li[2,6], D. Pei[7], A. J. Liang[2,6], P. Dudin[8], T. K. Kim[8], C. Cacho[8], Y. F. Xu[1], Y. Sun[5], L. X. Yang[9,10], Z. K. Liu[2,6], C. Felser[5,11,12], S. S. P. Parkin[1] and Y. L. Chen[2,6,7,9]✉

The spin–orbit coupling (SOC) lifts the band degeneracy that plays a vital role in the search for different topological states, such as topological insulators (TIs) and topological semimetals (TSMs). In TSMs, the SOC can partially gap a degenerate nodal line, leading to the formation of Dirac/Weyl semimetals (DSMs/WSMs). However, such SOC-induced gap structure along the nodal line in TSMs has not yet been systematically investigated experimentally. Here, we report a direct observation of such gap structure in a magnetic WSM $Co_3Sn_2S_2$ using high-resolution angle-resolved photoemission spectroscopy. Our results not only reveal the existence and importance of the strong SOC effect in the formation of the WSM phase in $Co_3Sn_2S_2$, but also provide insights for the understanding of its exotic physical properties.

npj Quantum Materials (2022)7:11 ; https://doi.org/10.1038/s41535-021-00392-9

INTRODUCTION

The spin–orbit coupling (SOC) effect originates from the relativistic interaction between a particle's spin and its orbital motion, which can modify atomic energy levels and split the energy bands in crystalline materials. The SOC effect is important in numerous research fields of physics, such as spintronics[1], ultracold atoms[2], high-temperature superconductivity[3,4], and topological materials[5–7]. In solids, it can lift the degeneracy of critical bands and play a vital role in the formation of exotic topological states[5–7]. As an example, in some topological materials, depending on how the SOC effect modifies the topological nodal line, different topological states can be formed: (i) the topological nodal line semimetals (TNLSMs) can be formed if the nodal line is not gapped[8,9]; (ii) the formation of topological insulators (TIs) if the nodal line is fully gapped[10–12]; (iii) if the nodal line is partially gapped with isolated nodal points, topological semimetals (TSMs) can be formed[13–21], such as Dirac semimetals (DSMs) or Weyl semimetals (WSMs).

In TIs and TSMs, the strength of SOC can be characterized by the energy gap size between the inverted bands and is dependent on the atomic mass. In compounds with heavy elements (e.g. bismuth-based TIs), the SOC-induced energy gap up to several hundred millielectron volts has been observed[22–25]. On the other hand, although many TSMs have been discovered[13–21,26–29] up to date, the SOC-induced gap structure along the nodal line has not yet been systematically investigated. However, the recently discovered magnetic WSM $Co_3Sn_2S_2$[18–21] provides an opportunity for such a study.

The WSM $Co_3Sn_2S_2$ has three pairs of Weyl points formed by partially gapped nodal lines due to the SOC effect;[20] which also give rise to giant anomalous Hall effect[18,19]. The scanning tunneling microscopy (STM) measurements observed a large negative flat band magnetism[30], spin–orbit polaron[31] and impurity-induced magnetic resonance[32] in $Co_3Sn_2S_2$ again indicate the effect of strong SOC in $Co_3Sn_2S_2$. Interestingly, a recent photoemission study[33] suggests the SOC effect in $Co_3Sn_2S_2$ is negligible and a degenerate Weyl loop state is formed.

In this report, we systematically investigate the SOC-induced gap structure along the nodal line in $Co_3Sn_2S_2$ using high-resolution angle-resolved photoemission spectroscopy (ARPES), and directly observed large SOC-induced energy gap (up to ~55 meV) distribution in the momentum space, which can be well reproduced by our ab initio calculations. These results clearly support the WSM nature, rather than the Weyl loop state in $Co_3Sn_2S_2$; which provide a solid electronic structure foundation for understanding many exotic physical properties in $Co_3Sn_2S_2$, such as the large anomalous Hall conductivity (AHC)[18,19], large anomalous Hall angle (AHA)[18], and anomalous Nernst effect (ANE)[34,35].

RESULTS

SOC effect in $Co_3Sn_2S_2$

$Co_3Sn_2S_2$ is crystallized in a trigonal rhombohedral structure and composed of stacked…-Sn-[S-(Co_3-Sn)-S]… layers (Fig. 1a). In each layer, Co atoms form a two-dimensional (2D) kagome lattice. Such a unique crystal structure guarantees the inversion symmetry, C_{3z} rotation symmetry and three mirror planes in $Co_3Sn_2S_2$. It undergoes a ferromagnetic (FM) transition at ~177 K[18,19]. The ab initio calculations on $Co_3Sn_2S_2$ in its FM state reveal a band inversion occurs near Fermi level (E_F)[20]. When SOC is ignored, the band inversion forms a nodal line as illustrated in Fig. 1c (see Supplementary Note 1 for more discussion) and totally six nodal lines locating in three mirror planes of the Brillouin zone (BZ) are formed (Fig. 1b). Each nodal line will be partially gapped when

[1]Max Planck Institute of Microstructure Physics, Halle 06120, Germany. [2]School of Physical Science and Technology, ShanghaiTech University, 201210 Shanghai, China. [3]Institute of Physics, Chinese Academy of Sciences, 100190 Beijing, China. [4]Songshan Lake Materials Laboratory, Dongguan, 523808 Guangdong, China. [5]Max Planck Institute for Chemical Physics of Solids, Dresden D-01187, Germany. [6]ShanghaiTech Laboratory for Topological Physics, 200031 Shanghai, China. [7]Clarendon Laboratory, Department of Physics, University of Oxford, Oxford OX1 3PU, UK. [8]Diamond Light Source, Didcot OX110DE, UK. [9]State Key Laboratory of Low Dimensional Quantum Physics, Department of Physics, Tsinghua University, 100084 Beijing, China. [10]Frontier Science Center for Quantum Information, 100084 Beijing, China. [11]John A. Paulson School of Engineering and Applied Sciences, Harvard University, Cambridge, MA 02138, USA. [12]Department of Physics, Harvard University, Cambridge, MA 02138, USA. [13]These authors contributed equally: D. F. Liu, E. K. Liu, Q. N. Xu. ✉email: yulin.chen@physics.ox.ac.uk

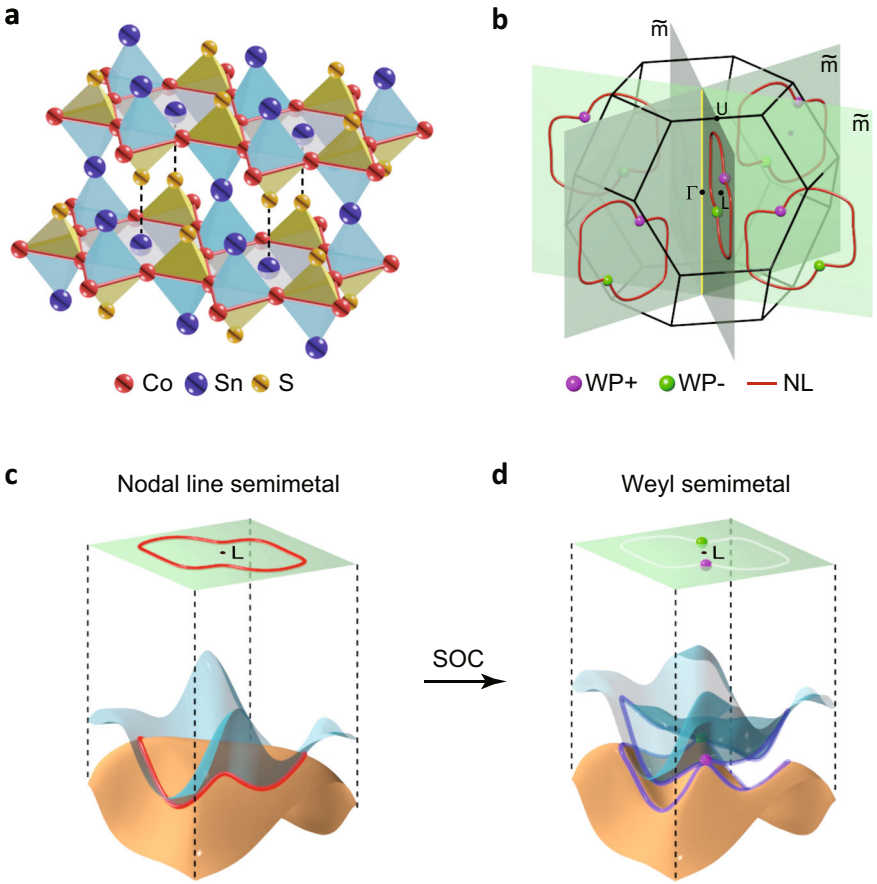

Fig. 1 Magnetic Weyl semimetal phase in $Co_3Sn_2S_2$. **a** The crystal structure of $Co_3Sn_2S_2$. **b** Schematic of the nodal line and Weyl points lying in three mirror planes of the bulk Brillouin zone. Red line represent the nodal line (NL) in the absence of the spin–orbit coupling (SOC) effect. In the presence of SOC, the nodal line will be partially gapped, leaving two nodal points forming the Weyl points (WPs) with positive (+, the magenta color point) and negative (−, the green color point) chirality, respectively. **c** Illustration of the nodal line originating from the band inversion in the absence of the SOC. **d** Illustration for the formation of the Weyl points and the partially gapped nodal line when SOC is included.

SOC is considered, leaving two nodal points in the formation of the Weyl points with opposite chiralities as illustrated in Fig. 1b, d.

To quantitatively visualize the position of the nodal line and the SOC effect on the nodal line, we first calculated the band dispersions along the $\bar{M}\prime - \bar{\Gamma} - \bar{M}$ direction with and without SOC as shown in Fig. 2c, d, respectively. Their momentum positions in the BZ are shown in Fig. 2a. Without SOC effect, the nodal line is characterized by the linear band crossings for all selected dispersions as shown by the black arrows in Fig. 2c. With changing the k_z value, the crossing point originally lies at ~50 meV above E_F [Fig. 2c (i, ii)], then moves down to ~ −50 meV below E_F [Fig. 2c (iii, iv)], and eventually moves up to ~ 100 meV above E_F [Fig. 2c (v, vi)]. Such behavior indicates the strong energy dispersion of the nodal line in the mirror plane. When SOC is considered, the crossing points are gapped as shown in Fig. 2d (i, iii–vi), while it remains nodal in Fig. 2d (ii) forming the Weyl point. We illustrate the SOC-induced energy gap size along the nodal line in Fig. 2b. It shows strong anisotropy ranging from 0 to ~50 meV. As ARPES probes the occupied states below E_F, the SOC-induced gap structure in Fig. 2d (iii, iv) can be observed experimentally. Based on the calculations, the portion of the gapped nodal line lying below E_F is marked by the cyan region as illustrated in Fig. 2a.

Observation of the SOC effect

To search for the gapped structure along the nodal line, we carried out detailed photon energy-dependent measurements along the $\bar{\Gamma}\,\bar{M}$ direction as shown in Fig. 3. The experimental dispersions taken at different photon energies are plotted in Fig. 3a. The measured position on the nodal line at different photon energies is illustrated by the black line in the inset of each panel. At the photon energy of 120 eV which accesses the $k_z = 0$ [Fig. 3a (i)] (see Supplementary Note 2 for more discussion), the gapped structure lies above E_F that can not be observed. Increasing the photon energy to 125 eV [Fig. 3a (ii)], the measured point on the nodal line lies in the cyan region [see the inset of Fig. 3a (ii)] indicating the gapped structure lying below E_F. Indeed, the corresponding gapped structure is clearly observed experimentally, characterized by the loss of intensity as illustrated by the arrow in Fig. 3a (ii). More photon energy-dependent measurements on different positions along the nodal line in the cyan region also resolve the SOC-induced gap structure [Fig. 3a (iii–vi)]. As the measured position moves out of the cyan region [see the inset of Fig. 3a (vii)], the gapped structure lies above E_F again. It is also confirmed by the experimental dispersion taken by 141 eV [Fig. 3a (vii)]. The energy distribution curves (EDCs) corresponding to Fig. 3a are shown in Fig. 3b. The SOC-induced gap is clearly visualized between the two branches of bands [Fig. 3b (ii–vi)] (see Supplementary Note 3 for more discussion).

We also carried out high-resolution measurements on the Fermi surface (FS) topology using the photon energy of 125 eV (Fig. 4a) and 134 eV (Fig. 4c) where the gapped nodal line lying below E_F. Both FS topologies exhibit a 3-fold symmetry which is consistent with the crystal structure. Three spot-like features were observed

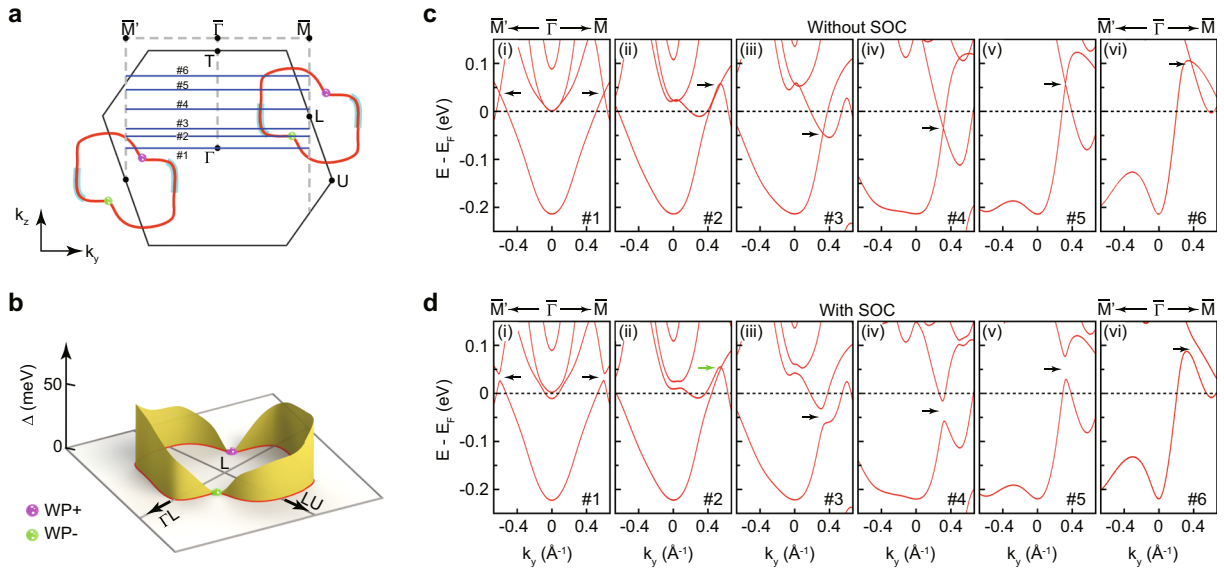

Fig. 2 The calculated band dispersions without and with SOC. a Illustration of the nodal line and Weyl points in one mirror plane. The cyan region of the nodal line represents the SOC-induced gap structure lying below E_F. **b** The calculated SOC-induced gap size along the nodal line. **c** The calculated band dispersions through the nodal line without SOC effect. Their momentum positions are shown by the blue lines in (**a**). The black arrows illustrate the nodal points along the nodal line. **d** The corresponding calculated band dispersions of (**c**) with SOC. The black arrows illustrate the gap opened by the SOC effect. The green arrow in (ii) illustrates the Weyl point. The calculated bandwidth was renormalized by a factor of 1.43 and the energy position was shifted to match the experiments.

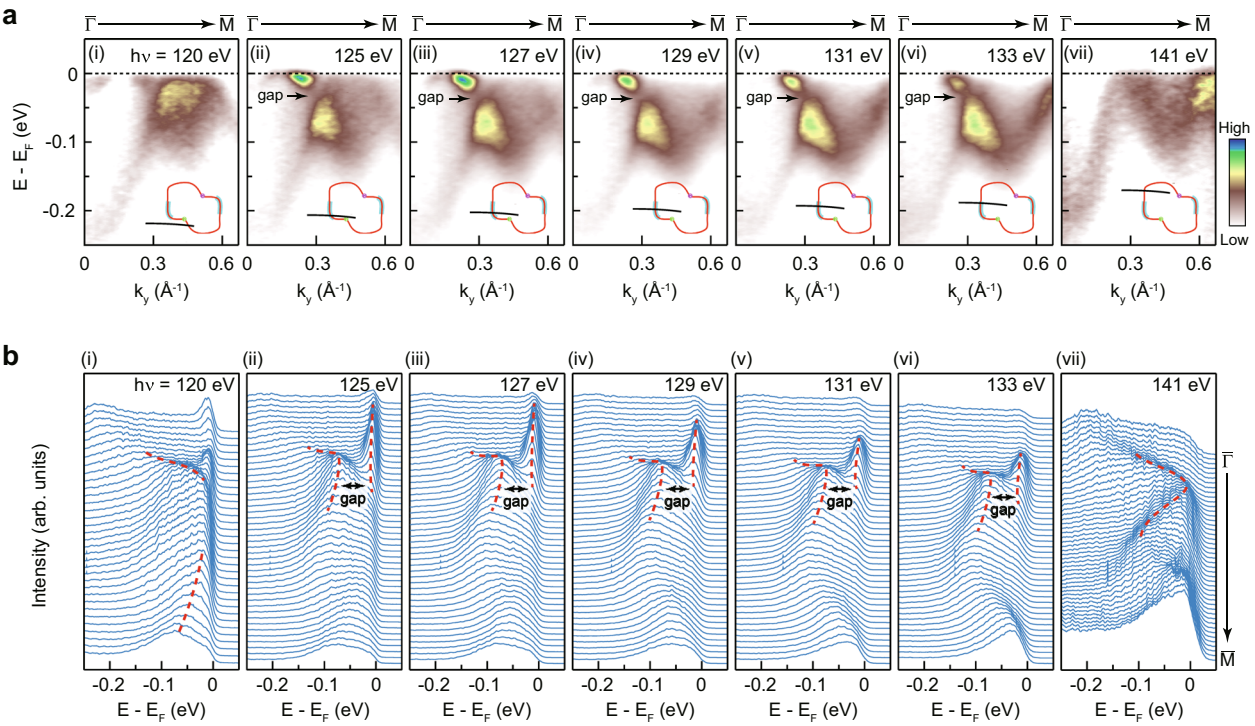

Fig. 3 Observation of the SOC-induced gap structure along the nodal line in $Co_3Sn_2S_2$. a The band structure along $\bar{\Gamma}\,\bar{M}$ direction taken at different photon energies. The measured position on the nodal line is marked by the black line in the inset of each panel. When the measured points locate out of the cyan region on the nodal line (i, vii), the gapped nodal line lies above E_F that can not be observed experimentally. Upon moving the measured point into the cyan region, the gapped nodal line lies below E_F, that are clearly observed experimentally as illustrated by the arrows in (ii–vi). **b** The corresponding energy distribution curves (EDCs) of (**a**). The SOC-induced gap is characterized by the separation of the two branches of bands in (ii–vi).

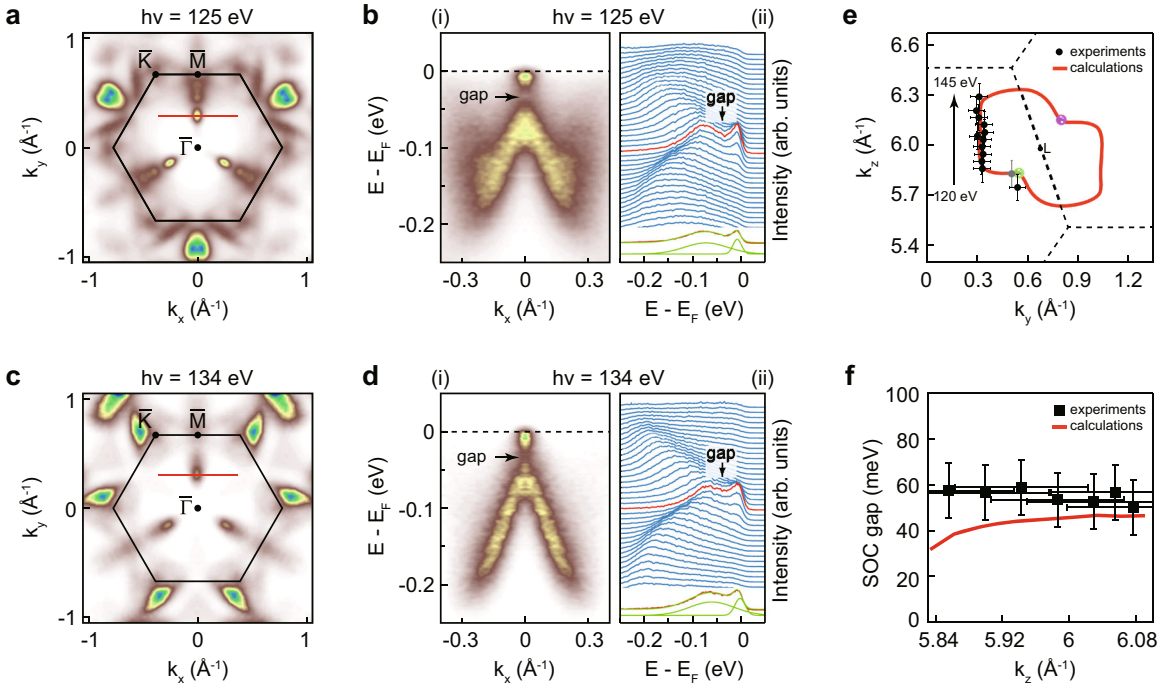

Fig. 4 SOC-induced gap size along the nodal line. a The Fermi surface topology taken at 125 eV photon energy. Three spot-like features are observed along $\bar{\Gamma}\bar{M}$ direction which originate from the upper branch of the gapped nodal line. **b** The extracted band structure (i) and its corresponding EDCs (ii) perpendicular to the $\bar{\Gamma}\bar{M}$ direction through the spot-like feature. The momentum path is illustrated by the red line in (**a**). The SOC-induced gap is clearly observed as illustrated by the arrow. To quantitatively extract the gap size, the EDC in red is fitted by using two Lorentzian curves as illustrated by the green curves in the inset of (ii). **c**, **d** The same to (**a**, **b**) but the data are taken at 134 eV photon energy. Note that the experimental plot has been symmetrized according to the crystal symmetry. **e** The extracted positions of nodal line. The gray point is taken by 115 eV photon energy and the position is obtained based on the inversion symmetrization. The experimental results show excellent agreement with the calculations. **f** The comparison of the SOC gap between the experiments and calculations shows overall consistency.

along the $\bar{\Gamma}\bar{M}$ direction on both FSs in the first BZ. These features originate from the upper branch of the gapped nodal line. In addition to the SOC-induced gap observed along the $\bar{\Gamma}\bar{M}$ direction (Fig. 3), we extracted the band dispersion through the spot-like feature perpendicular to the $\bar{\Gamma}\bar{M}$ direction as shown in Fig. 4b, d. Apparently, an energy gap developed between the upper and lower branch of the bands is clearly observed as illustrated by the arrows in Fig. 4b (i) and 4d (i). Such gap structure can also be seen from the EDCs, characterized by the two peaks structure with a dip in the middle [Fig. 4b (ii) and 4d (ii)].

By tracking the band dispersions, the position of the nodal line were determined experimentally as shown in Fig. 4e. It shows excellent agreement with the calculations. To quantitatively extract the SOC-induced gap size along the nodal line, we fit the two peaks of the EDCs by using two Lorentzian curves [see the insets of Fig. 4b (ii) and 4d (ii) for example]. The gap size is extracted by the energy interval between the two peaks and the results are shown in Fig. 4f. The gap size measured in the cyan region is around 55 meV, which is consistent with the calculations (Fig. 2b). The k_z independent gap size in Fig. 4f is mainly caused by the large k_z broadening effect[21].

DISCUSSION

The SOC-induced gap structure in $Co_3Sn_2S_2$ can help to understand the experimentally observed large AHC[18,19], large AHA[18] and the ANE[34,35]. The anomalous Hall effect in $Co_3Sn_2S_2$ is intrinsic that originates from the large Berry curvature[18], which will also enhance the thermoelectric response[34,35]. The calculations show the large Berry curvature arises mainly from the gapped region of the nodal line[18]. Our observations of the SOC-induced gap structure along the nodal line and the extracted positions of the nodal line show consistence with the calculations, suggesting that the formation of the gapped nodal line is essential for the large AHC[18,19], large AHA[18] and the ANE[34,35].

Compared with our results, the E_F in the previous work[33] lies at the top of the lower branch of the gapped nodal line, thus the SOC-induced gap structure lies above the E_F and can not be observed. Our results not only demonstrate the WSM nature of $Co_3Sn_2S_2$ with isolated Weyl points, rather than the degenerate Weyl loops, but also reveal the existence and importance of the strong SOC effect in the formation of the WSM phase in $Co_3Sn_2S_2$, as well as provide important insights for the understanding of many exotic physical properties in $Co_3Sn_2S_2$.

METHODS

High quality $Co_3Sn_2S_2$ single crystals were grown by self-flux method that can be found elsewhere. ARPES measurements were performed at beamline I05 of the Diamond Light Source (DLS) with a Scienta R4000 analyzer[36]. The angle resolution and overall energy resolution were better than 0.2° and 15 meV, respectively. The single crystals were cleaved in situ below 10 K. The pressure was kept below 2×10^{-10} Torr during the whole measurement.

DATA AVAILABILITY

The data of this study are available from the corresponding author upon reasonable request.

Received: 26 March 2021; Accepted: 16 October 2021;
Published online: 20 January 2022

REFERENCES

1. Zutic, I., Fabian, J. & Sarma, S. D. Spintronics: fundamentals and applications. *Rev. Mod. Phys.* **76**, 323 (2004).
2. Galitski, V. & Spielman, I. B. Spin-orbit coupling in quantum gases. *Nature* **49**, 49–54 (2013).
3. Borisenko, S. V. et al. Direct observation of spin-orbit coupling in iron based superconductors. *Nat. Phys.* **12**, 311–317 (2016).
4. Gotlieb, K. et al. Revealing hidden spin-momentum locking in a high-temperature cuprate superconductor. *Science* **362**, 1271–1275 (2018).
5. Qi, X.-L. & Zhang, S.-C. Topological insulators and superconductors. *Rev. Mod. Phys.* **83**, 1057 (2011).
6. Hasan, M. Z. & Kane, C. L. Colloquium: topological insulators. *Rev. Mod. Phys.* **82**, 3045 (2010).
7. Armitage, N. P., Mele, E. J. & Vishwanath, A. Weyl and Dirac semimetals in three-dimensional solids. *Rev. Mod. Phys.* **90**, 015001 (2018).
8. Bian, G. et al. Topological nodal-line fermions in spin-orbit metal $PbTaSe_2$. *Nat. Commnu* **7**, 10556 (2016).
9. Bian, G. et al. Drumhead surface states and topological nodal-line fermions in $TlTaSe_2$. *Phy. Rev. B* **93**, 121113 (R) (2016).
10. Yamakage, A. et al. Line-node Dirac semimetal and topological insulating phase in noncentrosymmetric pnictides CaAgX (X = P, As). *J. Phys. Soc. Jpn.* **85**, 013708 (2016).
11. Huang, H. et al. Topological nodal-line semiemtals in alkaline-earth stannides germanides, and silicides. *Phys. Rev. B* **93**, 201114 (R) (2016).
12. Xu, Q. et al. Topological nodal line semimetals in the CaP_3 family of materials. *Phys. Rev. B* **95**, 045136 (2017).
13. Weng, H. et al. Weyl semimetal phase in noncentrosymmetric transition-metal monophosphides. *Phys. Rev. X* **5**, 011029 (2015).
14. Huang, S.-M. et al. A Weyl Fermion semimetal with surface Fermi arcs in the transition metal monopnictide TaAs class. *Nat. Commun.* **6**, 7373 (2015).
15. Xu, S.-Y. et al. Discovery of a Weyl fermion semimetal and topological Fermi arcs. *Science* **349**, 613–617 (2015).
16. Lv, B. Q. et al. Experimental discovery of Weyl semimetal TaAs. *Phys. Rev. X* **5**, 031013 (2015).
17. Yang, L. X. et al. Weyl semimetal phase in the non-centrosymmetric compound TaAs. *Nat. Phys.* **11**, 728–732 (2015).
18. Liu, E. et al. Giant anomalous Hall effect in a ferromagnetic Kagome-lattice semimetal. *Nat. Phys.* **14**, 1125–1131 (2018).
19. Wang, Q. et al. Large intrinsic anomalous Hall effect in half-metallic ferromagnet $Co_3Sn_2S_2$ with magnetic Weyl fermions. *Nat. Commun.* **9**, 3681 (2018).
20. Xu, Q. et al. Topological surface Fermi arcs in the magnetic Weyl semimetal $Co_3Sn_2S_2$. *Phys. Rev. B* **97**, 235416 (2018).
21. Liu, D. F. et al. Magnetic Weyl semimetal phase in a Kagome crystal. *Science* **365**, 1282–1285 (2019).
22. Zhang, H. et al. Topological insulators in Bi_2Se_3, Bi_2Te_3 and Sb_2Te_3 with a single Dirac cone on the surface. *Nat. Phys.* **5**, 438–442 (2009).
23. Xia, Y. et al. Observation of a large-gap topological-insulator class with a single Dirac cone on the surface. *Nat. Phys.* **5**, 398–402 (2009).
24. Chen, Y. L. et al. Experimental realization of a three-dimensional topological insulator, Bi_2Te_3. *Science* **325**, 178–181 (2009).
25. Ando, Y. Topological insulator materials. *J. Phys. Soc. Jpn.* **82**, 102001 (2013).
26. Liu, Z. K. et al. Discovery of a three-dimensional topological Dirac semiemtal, Na_3Bi. *Science* **343**, 864–867 (2014).
27. Liu, Z. K. et al. A stable three-dimensional topological Dirac semiemtal Cd_3As_2. *Nat. Mater.* **13**, 677–681 (2014).
28. Yan, M. et al. Lorentz-violating type-II Dirac fermions in transition metal dichalcogenide $PtTe_2$. *Nat. Commun.* **8**, 257 (2017).
29. Jiang, J. et al. Signature of type-II Weyl semiemtal phase in $MoTe_2$. *Nat. Commun.* **8**, 13973 (2017).
30. Yin, J.-X. et al. Negative flat band magnetism in a spin-orbit-coupled correlated kagome magnet. *Nat. Phys.* **15**, 443–448 (2019).
31. Xing, Y. et al. Localized spin-orbit polaron in magnetic Weyl semimetal $Co_3Sn_2S_2$. *Nat. Commun.* **11**, 5613 (2020).
32. Yin, J.-X. et al. Spin-orbit quantum impurity in a topological magnet. *Nat. Commun.* **11**, 4415 (2020).
33. Belopolski, I. et al. Signatures of Weyl fermion annihilation in a correlated kagome magnet. *Phys. Rev. Lett.* **127**, 256403 (2021).
34. Guin, S. N. et al. Zero-field Nernst effect in a ferromagnetic Kagome-lattice Weyl-semiemtal $Co_3Sn_2S_2$. *Adv. Mater.* **31**, 1806622 (2019).
35. Ding, L. et al. Intrinsic anomalous Nernst effect amplified by disorder in a half-metallic semiemtal. *Phys. Rev. X* **9**, 041061 (2019).
36. Hoesch, M. et al. A facility for the analysis of the electronic structures of solids and their surfaces by synchrotron radiation photoelectron spectroscopy. *Rev. Sci. Instrum.* **88**, 013106 (2017).

ACKNOWLEDGEMENTS

E.K. Liu acknowledges the support from the National Natural Science Foundation of China (Nos. 52088101 and 11974394), National Key R&D Program of China (No. 2019YFA0704904) and the Strategic Priority Research Program (B) of the Chinese Academy of Sciences (No. XDB33000000). Z.K. Liu acknowledges the support from the National Key R&D program of China (Grants No.2017YFA0305400).

AUTHOR CONTRIBUTIONS

D.F.L., E.K.L., and Q.N.X. contributed equally to this work; Y.L.C. conceived the project. D.F.L. performed the ARPES experiments with the assistance of Y.W.L., D. P., A.J.L., and E.K.L. E.K.L. and J.L.S. synthesized the single crystals. Q.N.X. and Y.S. performed ab initio calculations. P. D., T.K.K., and C.C. provided the beamline support. Y.F.X., L.X.Y., Z.K.L., C.F. and S.S.P.P. contributed to the scientific discussions.

COMPETING INTERESTS

The authors declare no competing interests.

ADDITIONAL INFORMATION

Supplementary information The online version contains supplementary material available at https://doi.org/10.1038/s41535-021-00392-9.

Correspondence and requests for materials should be addressed to Y. L. Chen.

Reprints and permission information is available at http://www.nature.com/reprints

Publisher's note Springer Nature remains neutral with regard to jurisdictional claims in published maps and institutional affiliations.